Conference Note

tag: sPH-CONF-JET-2026-02
date: June 20, 2026

sPHENIX Conference Note

Jet production in Oxygen-Oxygen collisions at $\sqrt{s_{\mathrm{NN}}} = 200$ GeV with the sPHENIX detector

sPHENIX Collaboration

Abstract

This note reports the measurement of inclusive jet production in oxygen–oxygen (O+O) collisions at a nucleon–nucleon center–of–mass energy of $\sqrt{s_{\mathrm{NN}}}$ = 200 GeV, recorded with the sPHENIX detector at the Relativistic Heavy Ion Collider (RHIC) in 2026. Jets are reconstructed using the electromagnetic and hadronic calorimeters using the anti-k_t algorithm with a radius parameter of $R = 0.4$ in pseudorapidity $|\eta| < 0.7$ and transverse momentum (p_{T}) range of $19 < p_{\mathrm{T}} < 60$ GeV. The nuclear modification factor, R_{AA}, and the central-to-peripheral nuclear modification factor, R_{CP}, are measured as a function of jet p_{T} for several collision centrality intervals. The R_{CP} results are presented using two different peripheral event reference intervals. A clear centrality ordering is observed in both R_{AA} and R_{CP}, with the most central collisions showing the strongest suppression.

1 Introduction

A central goal of the high-energy heavy-ion program at the Relativistic Heavy Ion Collider (RHIC) and the Large Hadron Collider (LHC) is to characterize the quark–gluon plasma (QGP), the strongly interacting matter of deconfined quarks and gluons created at extreme temperatures and energy densities [1]. One of the most prominent features of the QGP is the energy loss of high-energy partons that traverse the produced medium, also known as jet quenching [2]. The magnitude of this energy loss is expected to depend on the medium energy density and in-medium path length [2, 3]. A direct experimental signature of jet quenching is the suppression of jet production in nucleus–nucleus collisions relative to expectations from an incoherent superposition of nucleon–nucleon collisions. This suppression is commonly quantified using the nuclear modification factor (R_{AA}) and the central-to-peripheral ratio (R_{CP}). The R_{AA} compares jet production in nucleus–nucleus collisions to that measured in p+p collisions, scaled by the nuclear overlap function (T_{AA}), while the R_{CP} compares jet production between central and peripheral nucleus–nucleus collisions, each scaled by the corresponding average number of binary nucleon–nucleon collisions (N_{coll}). These quantities are defined as

$$R_{AA} = \frac{1}{\langle T_{AA} \rangle} \frac{d^2 N_{\text{jet}}^{AA} / dp_{\text{T}} d\eta}{d^2 \sigma_{\text{jet}}^{pp} / dp_{\text{T}} d\eta}, \tag{1}$$

and

$$R_{CP} = \frac{1}{\langle N_{\text{coll}} \rangle} \frac{d^2 N_{\text{jet}}}{dp_{\text{T}}\, d\eta}\bigg|_{\text{central}} \Bigg/ \frac{1}{\langle N_{\text{coll}} \rangle} \frac{d^2 N_{\text{jet}}}{dp_{\text{T}}\, d\eta}\bigg|_{\text{peripheral}}, \tag{2}$$

where N_{jet} denotes the jet yield in a given transverse momentum (p_{T}) and pseudorapidity (η) interval. The nuclear overlap function is defined as

$$T_{AA} = \frac{N_{\text{coll}}}{\sigma_{NN}^{\text{inel}}}, \tag{3}$$

where $\sigma_{NN}^{\text{inel}}$ is the inelastic nucleon–nucleon cross section.

Oxygen–oxygen (O+O) collisions occupy a unique position in the system-size landscape, bridging the quark–gluon plasma (QGP) regime of large nucleus–nucleus (A+A) collisions, such as gold–gold (Au+Au) and lead–lead (Pb+Pb), and small systems including proton–proton (p+p) and proton–nucleus (p+A) collisions [4]. The intermediate system size of O+O collisions offers the opportunity to study jet quenching between large and small collision regimes, where the phenomenon is well established in A+A collisions but remains an open question in small systems [3]. In addition, compared to asymmetric p+A collisions, the symmetric collision geometry of O+O further reduces the initial-geometry uncertainties. Interest in O+O collisions has grown rapidly across both RHIC and the LHC [5, 6]. At RHIC, the STAR Collaboration reported results on hadron-triggered recoil jet yields at 200 GeV [7], showing a suppression of the yield in higher-activity events. At the LHC, the CMS experiment has observed suppressed charged-particle production in O+O collisions at 5.36 TeV [8], indicating significant jet quenching beyond cold nuclear matter effects. The ATLAS experiment reported the centrality-dependent dijet momentum imbalance in O+O relative to p+p collisions [9], with a modest modification of the momentum imbalance in central O+O collisions. No inclusive jet results in O+O collisions have been published at RHIC or the LHC to date.

This note presents measurements of the nuclear modification factor, R_{AA}, and the central-to-peripheral ratio, R_{CP}, for inclusive jets using data for O+O and p+p collisions at a nucleon–nucleon center–of–mass energy of $\sqrt{s_{\mathrm{NN}}}$ = 200 GeV. The analysis is performed across four O+O centrality intervals (0–20%, 20–40%, 40–60%, and 60–80%). Jets are reconstructed from the electromagnetic and hadronic calorimeters using the anti-k_t algorithm [10] with radius parameter $R = 0.4$. For the R_{CP} measurement, both the 40–60% and 60–80% intervals are used as peripheral references. The results for both R_{AA} and R_{CP} are reported as functions of jet p_{T} within $|\eta| < 0.7$ over the range $19 < p_{\mathrm{T}} < 60$ GeV.

2 The sPHENIX detector

sPHENIX [11, 12] is a multipurpose detector at RHIC designed to measure jet, heavy-flavor, and electromagnetic probes of the QGP, with a tracking system surrounded by electromagnetic and hadronic calorimetry inside and outside a 1.4 T superconducting solenoid. The measurements in this analysis use the full calorimeter system, which comprises the electromagnetic (EMCal) and hadronic (HCal) calorimeter subsystems, for jet reconstruction and the Level-1 (L1) trigger, and the Minimum Bias Detector (MBD) for triggering, vertex determination, and centrality estimation.

The calorimeter system has full azimuthal coverage and pseudorapidity acceptance $|\eta| < 1.1$. The EMCal is a tungsten–scintillating-fiber sampling calorimeter with a tower granularity $\Delta\eta \times \Delta\phi \approx 0.025 \times 0.025$, located inside the solenoid. The inner and outer HCal form an aluminum–scintillator and steel–scintillator sampling calorimeter, respectively, with individual tower size of $\Delta\eta \times \Delta\phi = 0.1 \times 0.1$. The combined response from EMCal and HCals measures the energy of the showers produced by the particles within a jet, and is the input to the jet-finding algorithm.

The MBD consists of two arrays of fast Cherenkov counters located at forward and backward rapidities ($3.51 < |\eta| < 4.61$) on both sides of the interaction region. It provides the minimum-bias trigger through a coincidence requirement between its two sides, the reconstructed collision z-vertex position along the beam direction, and the centrality estimation.

3 Data sample and event selection

The data used for O+O and p+p collisions were collected at $\sqrt{s_{\mathrm{NN}}}$ = 200 GeV in 2026 and 2024, respectively. Both datasets were taken under stable running conditions, with typical beam crossing angles of 0.75 mrad (O+O) and 1.5 mrad (p+p), resulting in narrow collision z-vertex distributions of $\sigma_z \approx 17$ cm and 13 cm, respectively. Events in O+O collisions are recorded using a jet trigger which requires an online calibrated transverse energy of at least 12 GeV on the L1 jet trigger primitive, in coincidence with the MBD requirement of at least one hit on both the forward and backward sides. The p+p analysis uses the same L1 jet trigger with a threshold of 10 GeV, without the MBD coincidence requirement.

A set of offline event selection criteria is applied by requiring events to have a reconstructed MBD z-vertex within $|v_z| < 60$ cm. For O+O collisions, events are required additionally to have at least one hit in an MBD photomultiplier on each side. The contribution from pileup is found to be less than 0.6% and therefore has a negligible impact on the O+O centrality intervals used in this analysis. The total integrated luminosity sampled in this analysis is 48.2 nb^{-1} and 21.3 pb^{-1} for O+O and p+p collisions, respectively.

The Monte Carlo (MC) samples used for the O+O analysis consist of PYTHIA-8 [13] hard-scattering jet events with the Detroit tune [14] embedded into O+O HIJING [15] events. A minimum-bias HIJING O+O sample is additionally used for event characterization and reweighting the simulation to reproduce the underlying-event conditions observed in data. For p+p collisions, the same PYTHIA-8 hard–scattering jet sample is used without HIJING embedding. The combined events are propagated through a full GEANT-4 [16] simulation of the sPHENIX detector and reconstructed in the same way as the data.

4 O+O centrality calibration

The collision centrality in O+O collisions is determined from the total charge sum measured in the MBD. The MBD charge-sum distribution in minimum-bias events is fitted with a convolution of a Monte Carlo (MC) Glauber model [6] and a negative binomial distribution (NBD), in which the sampled fraction of the total inelastic O+O cross section (1189 mb) is extracted and used to calibrate the centrality intervals. Figure 1 shows the measured MBD charge sum distribution compared to the best fit of MC Glauber $\oplus$ NBD. The dashed vertical line in the bottom panel indicates the MBD charge sum value above which the data are fully efficient and well described by the MC Glauber $\oplus$ NBD model. The inefficiency in peripheral collisions is studied by applying an efficiency correction to the measured yields, and is found to be sub-dominant compared to the systematic uncertainties on the Glauber variables. The geometric quantities including the mean N_{coll} used for computing the R_{CP} are evaluated for each centrality interval and summarized in Table 1.

Quantity	0–20%	20–40%	40–60%	60–80%
σ_{OO} (mb)		1189 ± 44		
$\langle N_{\text{part}} \rangle$	20.35 ± 0.38	12.76 ± 0.37	7.37 ± 0.24	4.16 ± 0.13
$\langle N_{\text{coll}} \rangle$	22.49 ± 0.94	12.16 ± 0.66	6.02 ± 0.33	2.92 ± 0.15
$\langle N_{\text{coll}} \rangle_X / \langle N_{\text{coll}} \rangle_{60\text{–}80\%}$	7.71 ± 0.219	4.17 ± 0.075	2.06 ± 0.035	—
$\langle N_{\text{coll}} \rangle_X / \langle N_{\text{coll}} \rangle_{40\text{–}60\%}$	3.74 ± 0.115	2.02 ± 0.027	—	—

Table 1: Summary of the Glauber variables for O+O collisions at $\sqrt{s_{\text{NN}}}$ =200 GeV. The uncertainties are the standard deviation over the 63 configurations (7 nuclear geometries $\times$ 3 σ_{NN} $\times$ 3 ω = 0.1, 0.3, 0.6).

For the uncertainty on the Glauber variables, a set of variations in the MC Glauber has been considered: 7 oxygen nuclear geometries, 3 nucleon–nucleon inelastic cross-section values (σ_{NN} = 40, 42, and 44 mb), and 3 values of ω ($\omega = 0.1, 0.3$, and 0.6), the shape parameter of the nucleon-nucleon overlap function, resulting in total 63 configurations. The standard deviation of these variations is taken as the systematic uncertainty for the Glauber variables [6].

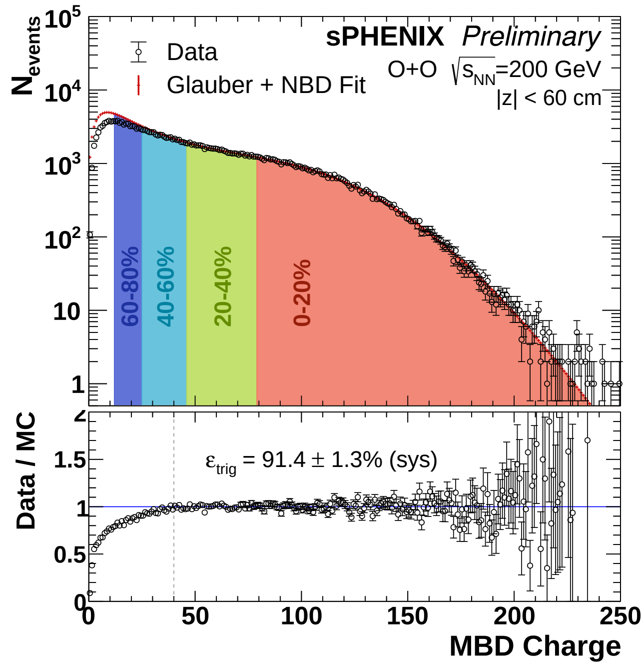

Figure 1: Distribution of the MBD charge sum in minimum-bias O+O collisions at $\sqrt{s_{NN}}$ = 200 GeV (points), compared to the best fit of the MC Glauber $\oplus$ NBD model (red line). The lower panel shows the data-to-fit ratio, with ϵ_{trig} representing the minimum-bias trigger efficiency. The dashed vertical line in the bottom panel indicates the MBD charge sum value above which the data are fully efficient.

5 Analysis procedure

The O+O and p+p data are analyzed using the same procedure, described in the following subsections: jet reconstruction, underlying-event (UE) subtraction, unfolding, and corrections.

5.1 Jet reconstruction and background rejection

Jets are reconstructed from EMCal and HCal towers using the anti-k_t algorithm with radius parameter $R = 0.4$. The underlying event (UE) contribution is determined event-by-event as an average energy density in η strips for each calorimeter layer, following an iterative procedure in which the constituent towers associated with identified jets are excluded from the calculation [17]. The estimated UE contribution is then subtracted from each measured jet. More details of the UE subtraction can be found in Ref. [18].

Beam-induced and non-collisional backgrounds are suppressed using the arrival timing information from the constituent calorimeter towers of each jet. The jet timing, computed as the energy-weighted mean tower time, is required to be within 2 ns of the collision time estimated from the MBD. Figure 2 shows the raw jet p_T spectra in O+O collisions after background rejection, for centrality intervals of 0–20%, 20–40%, 40–60%, 60–80%, and 0–100%. The spectra are given as counts normalized by the p_T^{calib} bin width, where p_T^{calib} denotes the reconstructed jet p_T after the jet energy scale correction.

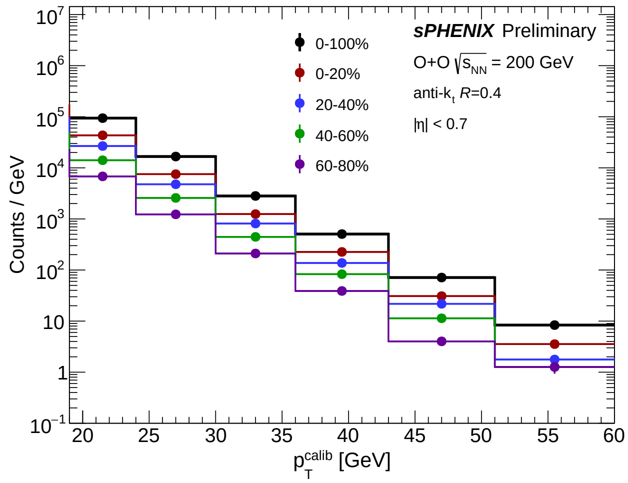

Figure 2: Raw jet p_T spectra in O+O collisions at $\sqrt{s_{NN}}$ = 200 GeV, after background rejection, for centrality intervals of 0–20%, 20–40%, 40–60%, 60–80%, and 0–100%. The spectra are given as counts normalized by the p_T^{calib} bin width.

In p+p collisions, additional selections are applied to further suppress these backgrounds. Events are required to contain a back-to-back dijet pair, with an azimuthal separation $\Delta\phi > 3\pi/4$ and the energy ratio between the subleading and leading jets greater than 0.3. Within the sPHENIX calorimetry acceptance the efficiency for this dijet requirement ranges from 62% to 92% over $19 < p_T < 60$ GeV, and is applied as a correction to the measured yields.

5.2 Jet energy scale and jet energy resolution

The jet energy scale (JES) and jet energy resolution (JER) are initially derived from the response of reconstructed to truth jets in MC simulation. Additional *in situ* corrections, obtained from p+p collision data, are then applied to account for differences in the jet response between data and simulation. The JES is calibrated using γ-jet and multijet transverse-momentum balance [19], while the JER is evaluated from the bisector and dijet-imbalance methods [20]. The use of these p+p-derived corrections in O+O collisions is validated by comparing the JES and JER in p+p and O+O simulation, which is found to be consistent once the underlying-event subtraction is included.

5.3 Corrections and unfolding

The measured jet p_T spectra are corrected for detector effects using a one-dimensional iterative Bayesian unfolding procedure, as implemented in the RooUnfold package [21, 22]. The response matrix of reconstructed and truth jets is constructed from the simulation, with the prior reweighted to describe the kinematic shape in data. The unmatched reconstructed and truth jets are taken into account as bin-by-bin purity and efficiency corrections, respectively. Figure 3 shows the response matrix of reconstructed and truth jets in O+O collisions from PYTHIA-8 + HIJING MC simulation for the 0–100% centrality interval.

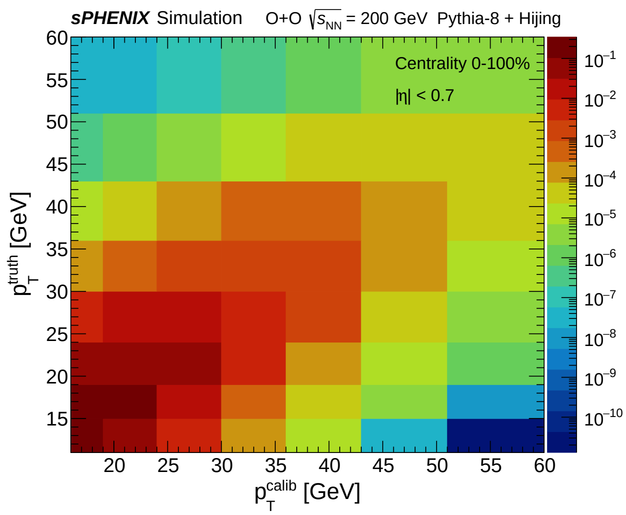

Figure 3: Response matrix for reconstructed and truth jets in O+O collisions from PYTHIA-8 + HIJING MC simulation for the centrality interval of 0–100%.

The unfolding procedure is validated through closure tests, in which simulated detector-level spectra are unfolded and compared with the corresponding truth-level distributions, using both the full simulation sample and statistically independent subsets of it. The number of iterations is optimized by balancing the stability across iterations against the growth of the statistical uncertainty. The statistical uncertainties are evaluated with a bootstrap method [23], in which the data and simulation are fluctuated according to their Poisson statistical uncertainties. In addition, a correction for the efficiency of the MBD coincidence requirement is evaluated as a function of the leading jet energy.

5.4 Systematic uncertainties

The sources considered for the systematic uncertainties include the JES and JER, the jet background removal procedure, the unfolding (from the prior reweighting and the number of iterations), the MBD efficiency, and the global uncertainties associated with the Glauber-model quantities. For each source, the full analysis chain is repeated under the corresponding variation, and the difference relative to the nominal result is taken as the systematic uncertainty. The total systematic uncertainty is obtained by summing the individual contributions in quadrature, separately, for the upward and downward variations.

For the JES, the *in situ* calibration is varied by its uncertainty as described in Ref. [19]. Similarly, the additional JER smearing is varied by its uncertainty from the bisector and dijet-imbalance methods described in Ref. [20].

The uncertainty on the background removal procedure described in Section 5.1 is estimated by tightening the jet-timing window around the MBD time from 2 ns to 1 ns. This accounts for residual non-collisional background that remains within the window, which is approximately uniform in time and distinct from the underlying event.

For the unfolding, two sources are considered and added in quadrature. The first source is the prior sensitivity, evaluated by varying the prior reweighting within its statistical uncertainty and repeating the unfolding procedure. The second is the sensitivity to the number of iterations, evaluated by performing one additional iteration beyond the optimal value used for the nominal result. The uncertainty in the MBD efficiency is evaluated using the data-driven efficiency alternatively to the nominal one which is obtained from simulation. The global uncertainties are evaluated with the MC Glauber variations summarized in Table 1.

For R_{CP}, each source is varied coherently and only the residual difference is taken as the systematic uncertainty. For R_{AA}, the JES and JER uncertainties are treated as fully correlated between O+O and p+p collisions, which partially cancels in the ratio, while the remaining sources are evaluated independently in the two systems and added in quadrature. Figure 4 summarizes the systematic uncertainties for R_{AA} in 0–100% centrality (left) and for R_{CP} in the 0–20%/40–60% centrality interval (right), showing the individual sources and the total uncertainty.

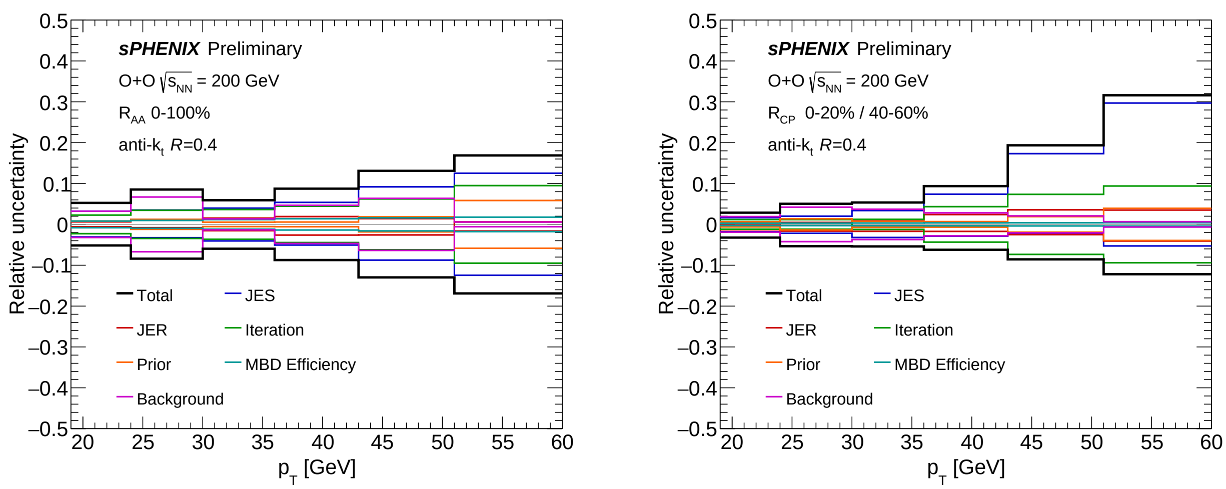

Figure 4: Summary of the systematic uncertainties on R_{AA} (left) and R_{CP} (right) as a function of jet p_T for the 0–100% and 0–20%/40–60% centrality intervals, respectively. The colored curves represent the individual sources and the black curve corresponds to the total systematic uncertainty.

6 Results

The jet nuclear modification factor, R_{AA}, is presented as a function of jet p_T. Figure 5 shows the R_{AA} results for $R = 0.4$ jets as a function of p_T in the 0–20%, 20–40%, 40–60%, and 60–80% centrality intervals (left) and in the inclusive 0–100% interval (right). A gradual decrease of R_{AA} is observed with increasing collision centrality. The R_{AA} hints at a decreasing trend with p_T, although consistent with no p_T dependence within statistical and systematic uncertainties. The centrality-integrated R_{AA} values are below unity, indicating a suppression of inclusive jet production in O+O collisions relative to the p+p reference.

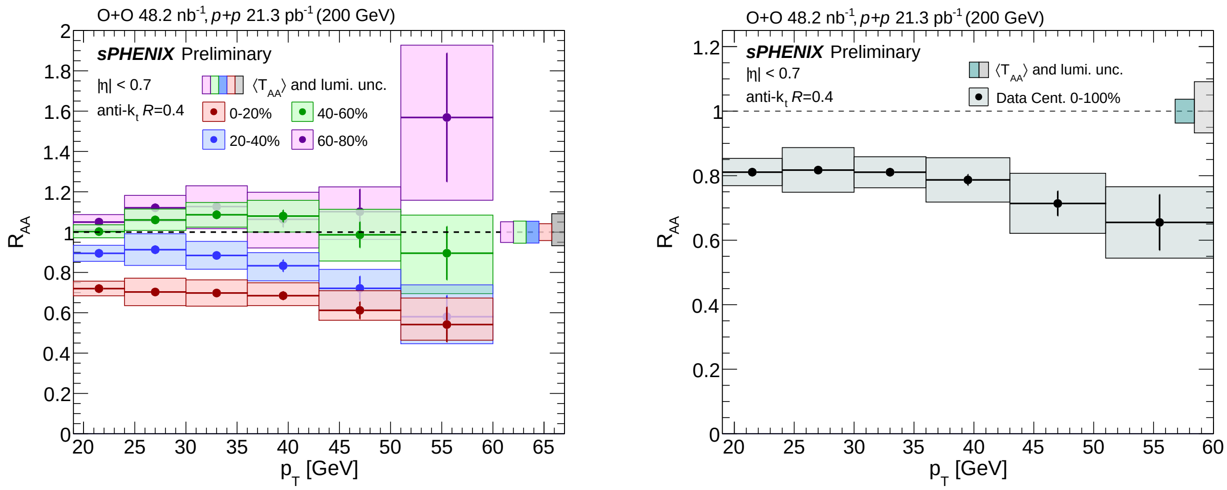

Figure 5: Jet R_{AA} as a function of jet p_{T} for O+O collisions at $\sqrt{s_{\mathrm{NN}}}$ = 200 GeV in the 0–20%, 20–40%, 40–60%, and 60–80% centrality intervals (left) and in the inclusive 0–100% interval (right). The vertical lines and boxes represent the statistical and systematic uncertainties, respectively.

Figure 6 shows the R_{AA} values compared with two theoretical calculations: one a baseline without jet-quenching effects, using several nuclear parton distribution functions (nPDFs) [5], and the other based on the Jewel (Jet Evolution With Energy Loss) version 2.4.0 MC generator [24, 25], shown both with and without recoils. The Jewel predictions are generated using the default configuration with an initial temperature T_i scaled with centrality via $T_i \propto \langle N_{\mathrm{part}} \rangle^{1/3}$, anchored at $T_i = 0.26$ GeV for the 0–20% centrality interval. This anchored temperature is derived from hydrodynamic simulation results in Ref. [26]. The PDF used for the Jewel simulation is CT10 NLO, with no nPDF incorporated. Overall, the R_{AA} values lie below the baseline nPDF calculations, but remain consistent with them within one standard deviation. The effect of recoils in the Jewel simulation is found to be modest, at most 10%, with both variants consistent with the measured R_{AA}.

Measurements of the jet central-to-peripheral nuclear modification factor (R_{CP}) are performed using two different peripheral reference intervals, 40–60% and 60–80%. Employing different references allows for a systematic check on the relative modification across centrality, with the 40–60% reference offering higher statistics and reduced uncertainties. Figure 7 shows the results for R_{CP} with the peripheral reference taken as the 60–80% centrality interval (left) and as the 40–60% interval (right). The measured R_{CP} values indicate a decrease at high p_{T}, while the present uncertainties prevent a firm conclusion. A suppression is observed in the 0–20% and 20–40% intervals for both references, with the 0–20% interval being more suppressed. Relative to the 60–80% reference, the R_{CP} values for the 40–60% interval are consistent with unity, indicating no additional modification.

To account for potential centrality bias effects, which arise from the correlation between hard processes and the soft particle production used in the centrality determination [27], the measured R_{CP} values are compared to the predicted bias factors from the Angantyr MC generator [28]. Figure 8 shows the R_{CP} values overlaid with the central-to-peripheral ratio of the bias factors for the corresponding centrality intervals. The bias factors on the R_{CP} are found to deviate from unity by less than 10% across the studied p_{T} range. This shows that the suppression found in the

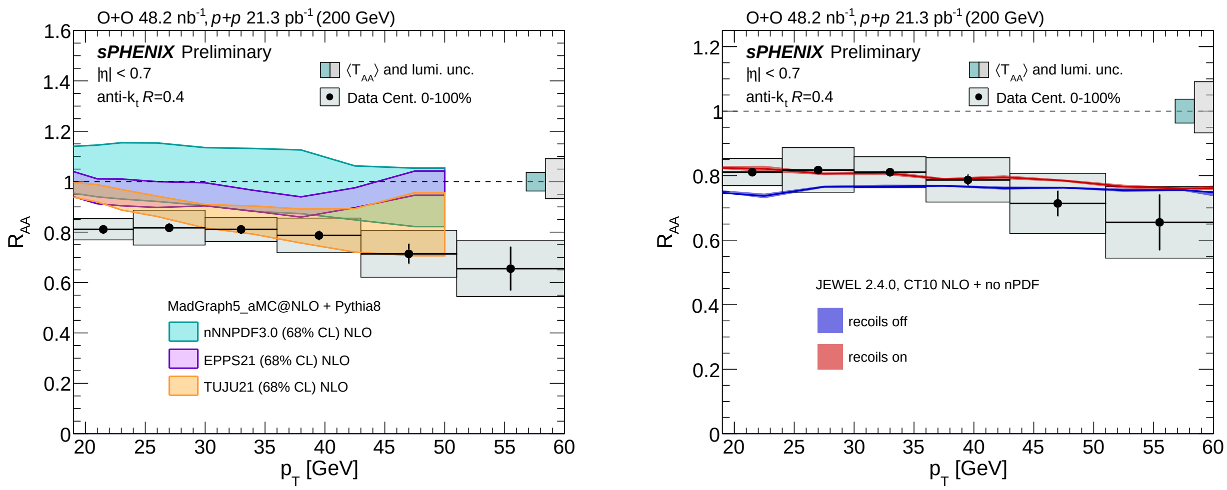

Figure 6: Jet R_{AA} as a function of jet p_{T} for O+O collisions at $\sqrt{s_{\mathrm{NN}}} = 200$ GeV in the 0–100% centrality intervals compared to baseline calculations with three nPDFs (left) and to predictions from Jewel (right). The vertical lines and boxes represent the statistical and systematic uncertainties, respectively.

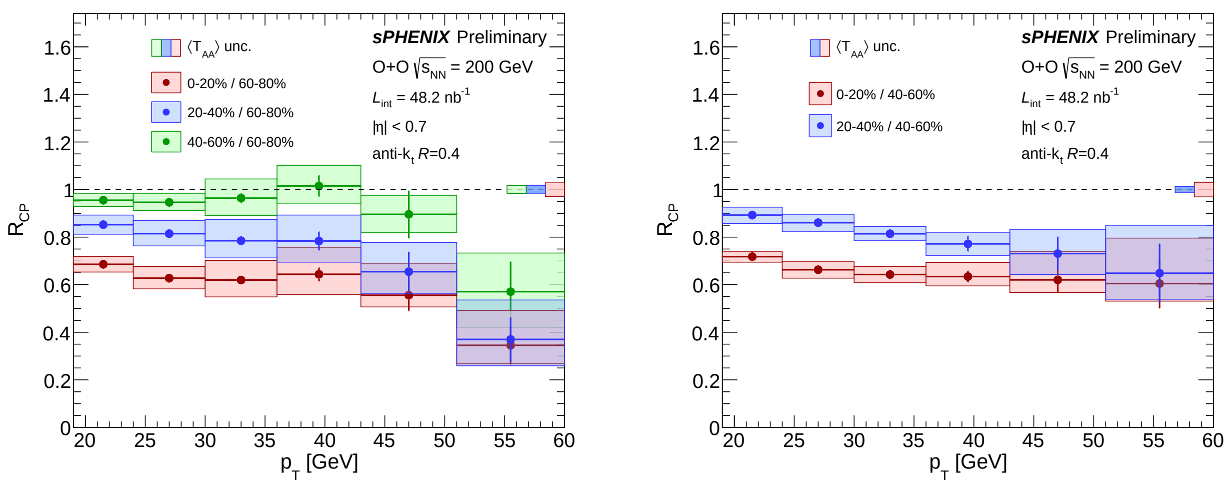

Figure 7: Jet R_{CP} as a function of jet p_{T} for O+O collisions at $\sqrt{s_{\mathrm{NN}}} = 200$ GeV, with the peripheral reference taken as the 60–80% centrality interval (left) and the 40–60% centrality interval (right). The red, blue, and green colors correspond to the selected centrality interval 0–20%, 20–40%, and 40–60%. The vertical lines and boxes represent the statistical and systematic uncertainties, respectively. The boxes at unity show the systematic uncertainties for the N_{coll} values.

R_{CP} values for 0–20% and 20–40% is beyond centrality bias effects, supporting the presence of jet quenching effects in O+O collisions.

Figures 9 and 10 show the measured R_{CP} values for the 60–80% and 40–60% peripheral reference intervals, respectively, compared to predictions from Jewel without (left) and with (right) recoils. The predictions are in agreement with the data within uncertainties.

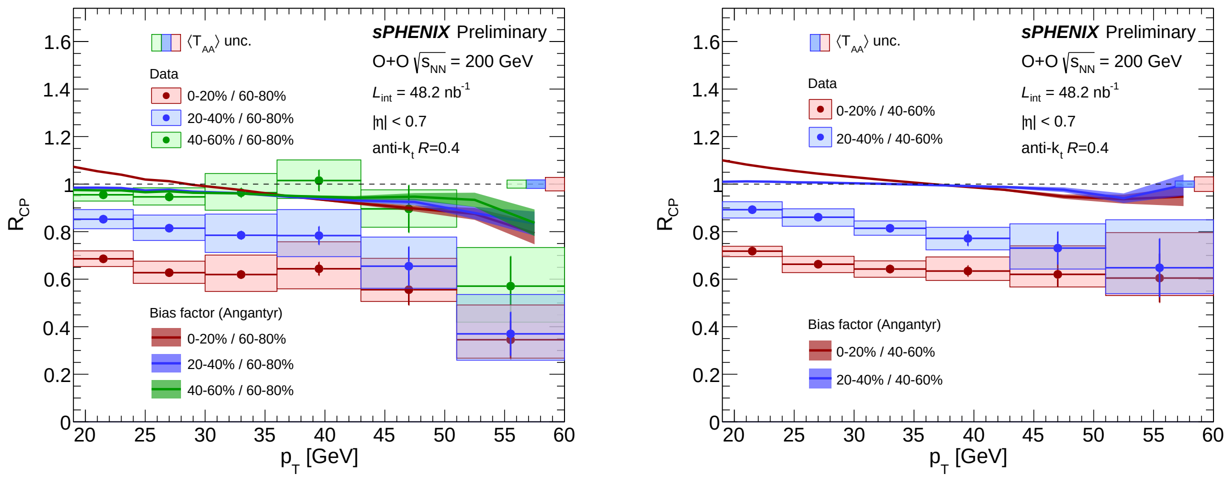

Figure 8: Jet R_{CP} as a function of jet p_T for O+O collisions at $\sqrt{s_{NN}}$ = 200 GeV, with the peripheral reference taken as the 60–80% centrality interval (left) and the 40–60% centrality interval (right). The red, blue, and green colors correspond to the selected centrality interval 0–20%, 20–40%, and 40–60%. The vertical lines and boxes represent the statistical and systematic uncertainties, respectively. The boxes at unity show the systematic uncertainties for the N_{coll} values. The bands represent the bias factors from ANGANTYR simulation.

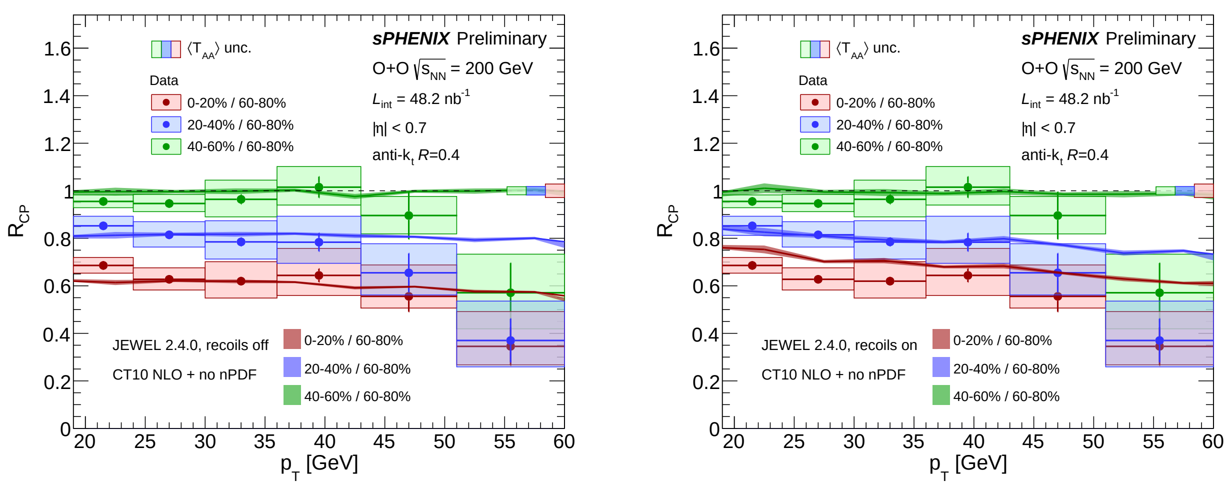

Figure 9: Jet R_{CP} as a function of jet p_T for O+O collisions at $\sqrt{s_{NN}}$ = 200 GeV, with the peripheral reference taken as the 60–80% centrality interval. The red, blue, and green colors correspond to the 0–20%, 20–40%, and 40–60% centrality intervals, respectively. The vertical lines and boxes represent the statistical and systematic uncertainties, respectively. The boxes at unity show the systematic uncertainties for the N_{coll} values. The bands represent the theoretical predictions from JEWEL without (left) and with (right) recoils enabled.

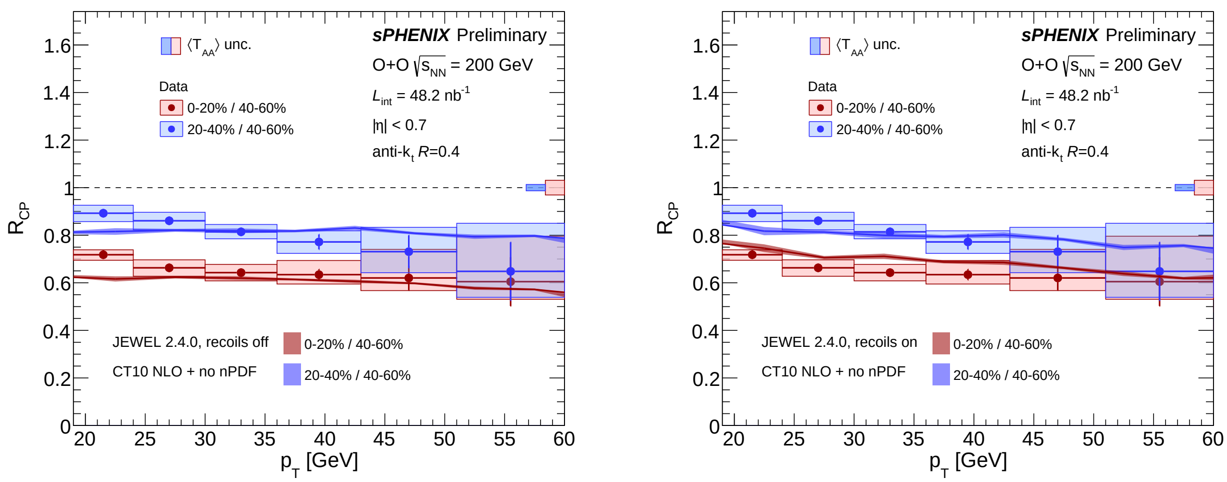

Figure 10: Jet R_{CP} as a function of jet p_{T} for O+O collisions at $\sqrt{s_{\mathrm{NN}}}$ = 200 GeV, with the peripheral reference taken as the 40–60% centrality interval. The red and blue colors correspond to the 0–20% and 20–40% centrality intervals, respectively. The vertical lines and boxes represent the statistical and systematic uncertainties, respectively. The boxes at unity show the systematic uncertainties for the N_{coll} values. The bands represent the predictions modeled by Jewel without (left) and with (right) recoils.

7 Summary

This note reports the measurement of the nuclear modification factor, R_{AA}, and the central-to-peripheral nuclear modification factor, R_{CP}, for inclusive jets using O+O and p+p data at $\sqrt{s_{\mathrm{NN}}}$ = 200 GeV, recorded by the sPHENIX detector at RHIC in 2026 and 2024, respectively. Jets are reconstructed using the electromagnetic and hadronic calorimeters with the anti-k_t algorithm using a radius parameter $R = 0.4$. The R_{AA} and R_{CP} results are presented as functions of transverse momentum (p_{T}) within $|\eta| < 0.7$. For the R_{CP} measurement, two peripheral reference intervals (40–60% and 60–80%) are considered. A clear centrality dependence is observed in both observables, with stronger suppression found in more central collisions. The magnitude of the suppression exceeds the contribution from centrality bias effects. The results are also compared with theoretical predictions that incorporate jet-quenching effects and are found to be consistent within uncertainties. These findings provide evidence for jet quenching in O+O collisions at RHIC energies, and establish an important point of comparison with measurements in other collision systems and at different collision energies. Together, these results are expected to constrain the properties of the medium across the system-size landscape from small systems to large nucleus–nucleus collisions.

References

[1] Wit Busza, Krishna Rajagopal, and Wilke van der Schee. Heavy Ion Collisions: The Big Picture, and the Big Questions. *Ann. Rev. Nucl. Part. Sci.*, 68:339, 2018. arXiv:1802.04801, doi:10.1146/annurev-nucl-101917-020852. 1

[2] Leticia Cunqueiro and Anne M. Sickles. Studying the QGP with Jets at the LHC and RHIC. *Prog. Part. Nucl. Phys.*, 124:103940, 2022. arXiv:2110.14490, doi:10.1016/j.ppnp.2022.103940. 1

[3] A. Huss et al. Predicting parton energy loss in small collision systems. *Phys. Rev. C*, 103:054903, 2021. arXiv:2007.13758, doi:10.1103/PhysRevC.103.054903. 1, 1

[4] Jasmine Brewer, Aleksas Mazeliauskas, and Wilke van der Schee. Opportunities of OO and pO collisions at the LHC. 3 2021. arXiv:2103.01939. 1

[5] Jannis Gebhard, Aleksas Mazeliauskas, and Adam Takacs. No-quenching baseline for energy loss signals in oxygen-oxygen collisions. *JHEP*, 04:034, 2025. arXiv:2410.22405, doi:10.1007/JHEP04(2025)034. 1, 6

[6] Constantin Loizides. Glauber predictions for oxygen and neon collisions at energies available at the CERN Large Hadron Collider. *Phys. Rev. C*, 113(1):014914, 2026. arXiv:2507.05853, doi:10.1103/mkp8-zgxh. 1, 4, 4

[7] STAR Collaboration. Measurement of jet quenching in O+O collisions at $\sqrt{s_{\mathrm{NN}}} = 200$ GeV by the STAR experiment at RHIC. 4 2026. arXiv:2604.13935. 1

[8] CMS Collaboration. Observation of Suppressed Charged-Particle Production in Ultrarelativistic Oxygen-Oxygen Collisions. *Phys. Rev. Lett.*, 136(16):162301, 2026. arXiv:2510.09864, doi:10.1103/89sf-9t1x. 1

[9] ATLAS Collaboration. Observation of centrality-dependent dijet transverse momentum imbalance in O+O and Ne+Ne collisions at $\sqrt{s_{NN}} = 5.36$ TeV with the ATLAS detector. 6 2026. arXiv:2606.20463. 1

[10] Matteo Cacciari, Gavin P. Salam, and Gregory Soyez. The anti-k_t jet clustering algorithm. *JHEP*, 04:063, 2008. arXiv:0802.1189, doi:10.1088/1126-6708/2008/04/063. 1

[11] A. Adare et al. An Upgrade Proposal from the PHENIX Collaboration. 2015. arXiv:1501.06197. 2

[12] R. Belmont et al. Predictions for the sPHENIX physics program. *Nucl. Phys. A*, 1043:122821, 2024. doi:10.1016/j.nuclphysa.2024.122821. 2

[13] Torbjörn Sjöstrand et al. An Introduction to PYTHIA 8.2. *Comput. Phys. Commun.*, 191:159, 2015. arXiv:1410.3012, doi:10.1016/j.cpc.2015.01.024. 3

[14] Manny Rosales Aguilar, Zilong Chang, Raghav Kunnawalkam Elayavalli, Renee Fatemi, Yang He, Yuanjing Ji, Dmitry Kalinkin, Matthew Kelsey, Isaac Mooney, and Veronica Verkest. PYTHIA8 underlying event tune for RHIC energies. *Phys. Rev. D*, 105(1):016011, 2022. arXiv:2110.09447, doi:10.1103/PhysRevD.105.016011. 3

[15] Xin-Nian Wang and Miklos Gyulassy. HIJING: A Monte Carlo model for multiple jet production in pp, pA and AA collisions. *Phys. Rev. D*, 44:3501, 1991. doi:10.1103/PhysRevD.44.3501. 3

[16] S. Agostinelli et al. GEANT4–a simulation toolkit. *Nucl. Instrum. Meth. A*, 506:25, 2003. doi:10.1016/S0168-9002(03)01368-8. 3

[17] J. A. Hanks, A. M. Sickles, B. A. Cole, A. Franz, M. P. McCumber, D. P. Morrison, J. L. Nagle, C. H. Pinkenburg, B. Sahlmueller, P. Steinberg, M. von Steinkirch, and M. Stone. Method for separating jets and the underlying event in heavy ion collisions at the bnl relativistic heavy ion collider. *Phys. Rev. C*, 86:024908, 2012. URL: `https://link.aps.org/doi/10.1103/PhysRevC.86.024908`, `doi:10.1103/PhysRevC.86.024908`. 5.1

[18] sPHENIX Collaboration. Measurement of dijet momentum balance in Au+Au collisions at $\sqrt{s_{\mathrm{NN}}}$ = 200 GeV with the sPHENIX detector. sPHENIX Conference Note sPH-CONF-JET-2025-05, 2025. URL: `https://www.sphenix.bnl.gov/PublicResults/sPH-CONF-JET-2025-05`. 5.1

[19] sPHENIX Collaboration. Precise measurement of jet energy scale derived from in situ techniques using γ-jet and multijet transverse momentum balance in p+p collisions at $\sqrt{s}$ = 200 GeV with the sPHENIX detector. sPHENIX Conference Note sPH-CONF-JET-2026-01, 2026. URL: `https://www.sphenix.bnl.gov/PublicResults/sPH-CONF-JET-2026-01`. 5.2, 5.4

[20] sPHENIX Collaboration. Measurement of dijet transverse momentum imbalance and azimuthal acoplanarity in p+p collisions at $\sqrt{s}$ = 200 GeV with the sPHENIX detector. 2026. `arXiv:2606.17184`. 5.2, 5.4

[21] G. D'Agostini. A Multidimensional unfolding method based on Bayes' theorem. *Nucl. Instrum. Meth. A*, 362:487–498, 1995. `doi:10.1016/0168-9002(95)00274-X`. 5.3

[22] Tim Adye. Unfolding algorithms and tests using RooUnfold. In *PHYSTAT 2011*, pages 313–318, Geneva, 2011. CERN. `arXiv:1105.1160`, `doi:10.5170/CERN-2011-006.313`. 5.3

[23] Evaluating statistical uncertainties and correlations using the bootstrap method. Technical report, CERN, Geneva, 2021. All figures including auxiliary figures are available at https://atlas.web.cern.ch/Atlas/GROUPS/PHYSICS/PUBNOTES/ATL-PHYS-PUB-2021-011. URL: `https://cds.cern.ch/record/2759945`. 5.3

[24] Korinna Zapp, Gunnar Ingelman, Johan Rathsman, Johanna Stachel, and Urs Achim Wiedemann. A Monte Carlo Model for 'Jet Quenching'. *Eur. Phys. J. C*, 60:617–632, 2009. `arXiv:0804.3568`, `doi:10.1140/epjc/s10052-009-0941-2`. 6

[25] Korinna C. Zapp. JEWEL 2.0.0: directions for use. *Eur. Phys. J. C*, 74(2):2762, 2014. `arXiv:1311.0048`, `doi:10.1140/epjc/s10052-014-2762-1`. 6

[26] M. Habich, J. L. Nagle, and P. Romatschke. Particle spectra and HBT radii for simulated central nuclear collisions of C + C, Al + Al, Cu + Cu, Au + Au, and Pb + Pb from $\sqrt{s}$ = 62.4 - 2760 GeV. *Eur. Phys. J. C*, 75(1):15, 2015. `arXiv:1409.0040`, `doi:10.1140/epjc/s10052-014-3206-7`. 6

[27] JaeBeom Park, J. L. Nagle, Dennis V. Perepelitsa, Sanghoon Lim, and Constantin Loizides. Selection-bias effects on high-p_T yield and correlation measurements in oxygen+oxygen collisions. *Phys. Rev. C*, 112:064916, 2025. `arXiv:2507.03603`, `doi:10.1103/yr6k-97mn`. 6

[28] Bierlich, Christian and Gustafson, Gösta and Lönnblad, Leif and Shah, Harsh. The Angantyr model for heavy-ion collisions in PYTHIA8. *JHEP*, 10:134, 2018. `arXiv:1806.10820`, `doi:10.1007/JHEP10(2018)134`. 6

A Model comparisons

This section compares the results to the bias factors and predictions from Jewel in different centrality intervals.

Figure 11 shows the R_{CP} values for the reference intervals 40–60% and 60–80%, overlaid with the effect from the bias factors calculated using Angantyr simulation.

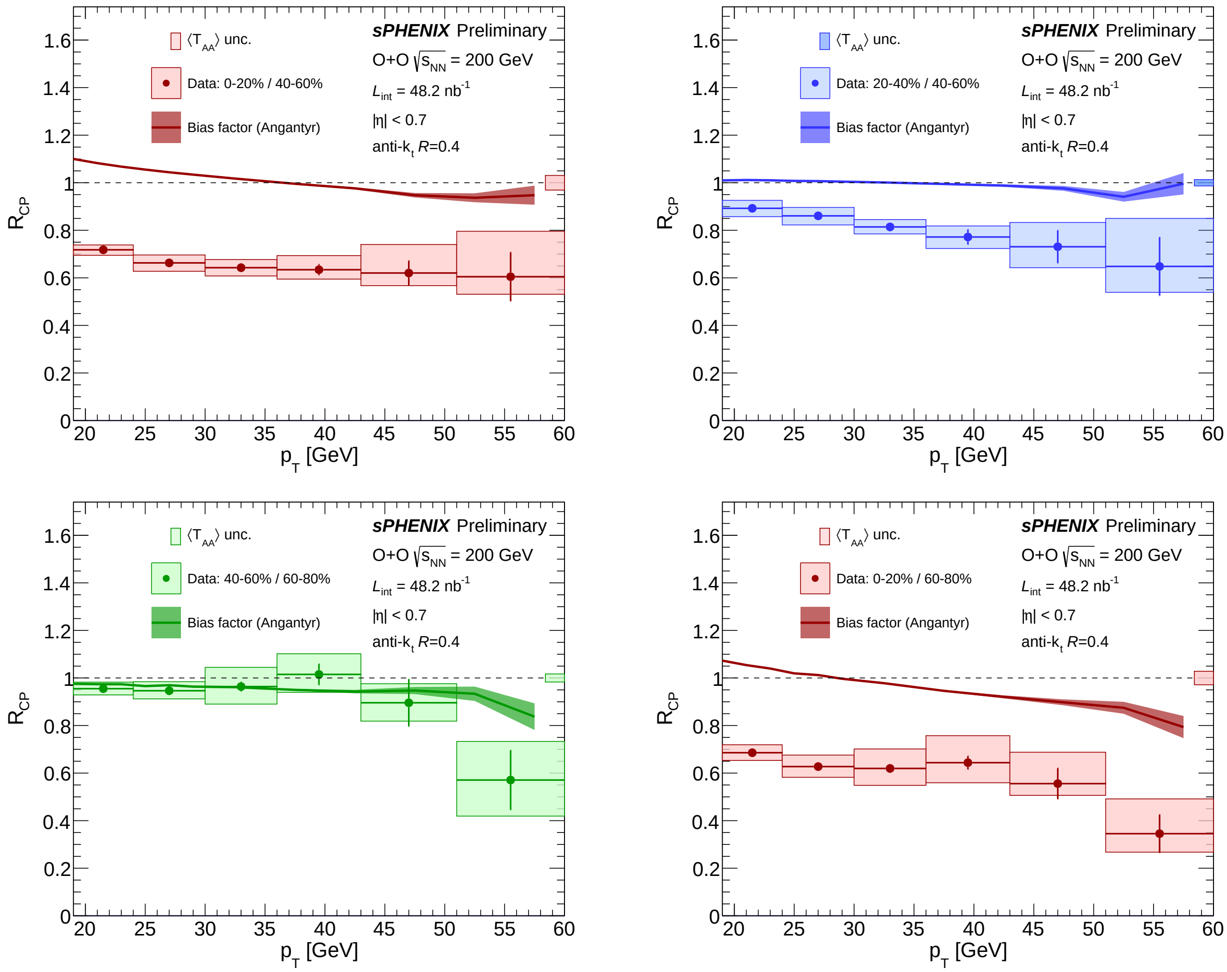

Figure 11: Jet R_{CP} as a function of jet p_{T} for O+O collisions at $\sqrt{s_{\mathrm{NN}}}$ = 200 GeV for the reference centrality intervals of 40–60% (top) and 60–80% (bottom). The vertical lines and boxes represent the statistical and systematic uncertainties, respectively. The bands represent the effects of the bias factors obtained from Angantyr simulation.

Figure 12 shows the R_{AA} results compared to Jewel predictions for centrality intervals of 0–20%, 20–40%, 40–60% and 60–80%.

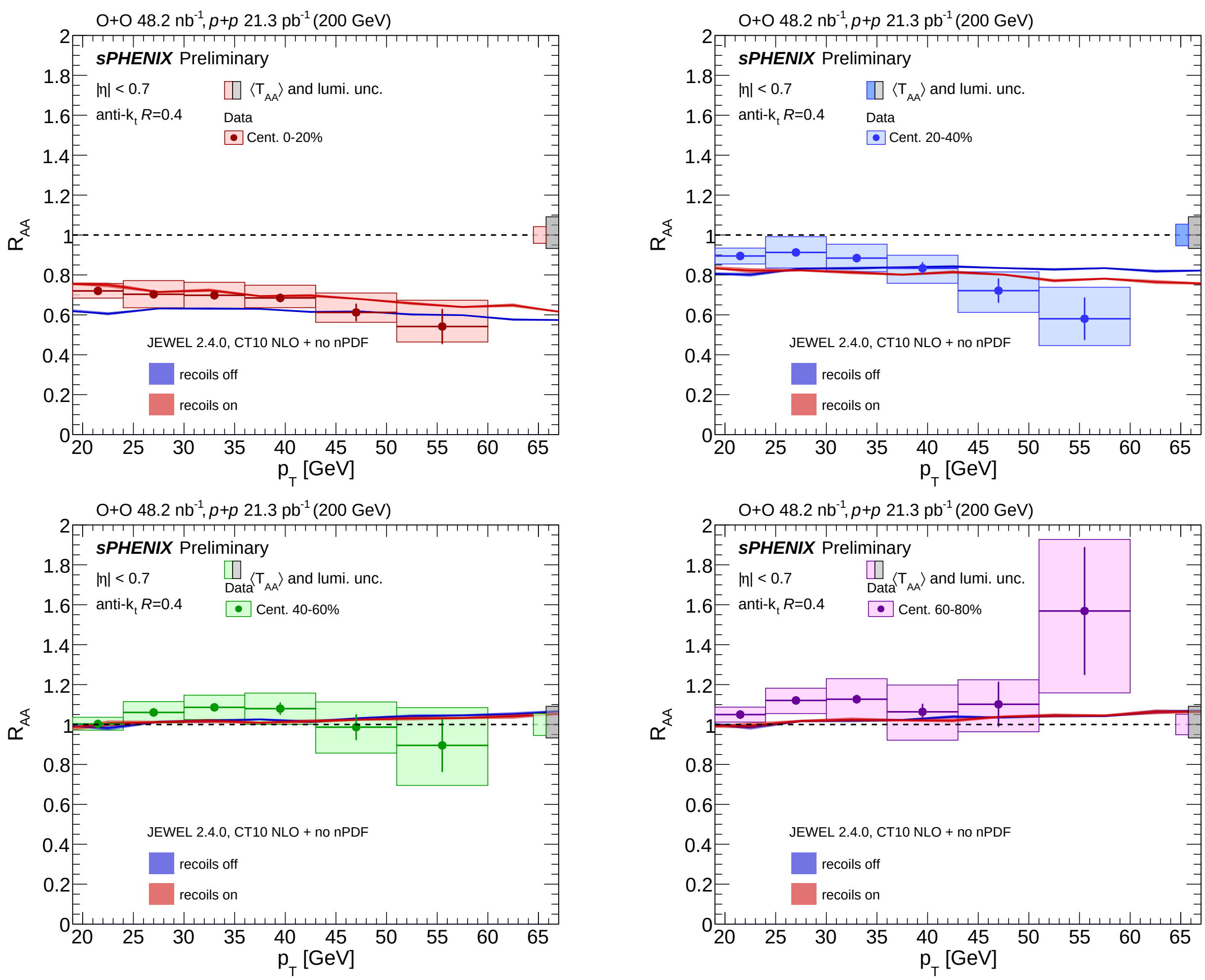

Figure 12: Jet R_{AA} as a function of jet p_T for O+O collisions at $\sqrt{s_{NN}}$ = 200 GeV in centrality intervals of 0–20%, 20–40%, 40–60%, and 60–80%. The vertical lines and boxes represent the statistical and systematic uncertainties, respectively. The red and blue bands represent the theoretical predictions from JEWEL with and without recoils enabled.